OPTICAL DESIGN FOR BIPM IMAGING SYSTEM

D. Kramer, B. Dehning, C. Fischer, S. Hutchins, J. Koopman, CERN, Geneva, Switzerland

Abstract

The light imaging system for the Beam Ionization Profile Monitor (BIPM) was designed to allow simultaneous operation of a fast Multi Anode Photo Multiplier and two new types of intensified standard resolution CCD cameras.

The main reason for designing the optics was the poor resolution of the preliminary setup limiting seriously the detectors performance and the need of a second optical path for the Multi (32) Anode Photo Multiplier (MAPMT). An increase of the optical luminosity was also necessary for low intensity beams. Optimization of the optical system was done in the ZEMAX program.

The imaging error was checked by comparing the ionization profile monitor continuous measurements with wire scanner measurements.

INTRODUCTION

The BIPM uses the rest gas in the vacuum beam pipe as ionizing medium where electrons are produced during every beam passage. These electrons are accelerated in a uniform vertical or horizontal electric field and are forced to spiral along the magnetic field lines, which are parallel to the electric field. The Electrons are multiplied by means of an MCP and subsequently hit a phosphor plate get converted into photons.

The density profile of the beam is transformed to the spatial distribution of the photons. The image formed on the phosphor plate has to be properly imaged to a CCD and MAPMT placed outside of the vacuum tank. A new Imaging System (Fig. 1) was designed for the detector.

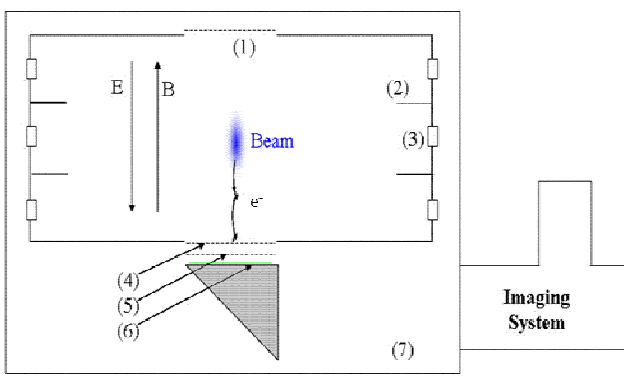

(1)…HV Cathode grid
(2)…Field homogenization electrodes
(3)…Resistors
(4)…Multi-Channel Plate (MCP_{in}) entrance electrode
(5)…MCP_{out} exit electrode
(6)…Phosphor plate deposited on indium tin oxide and fused silica reflecting optical prism
(7)…Vacuum tank

Figure 1: BIPM detector schematics.

DESIGN TARGETS

The main design parameter was the paraxial magnification. It was calculated simply as *m = image size / object size*. Object size was the length of the phosphor screen and for the image, the shortest side of the larger CCD element was used.

Maximal lens diameter was fixed to 50.2 mm due to the width of the viewing port in the IPM dipole magnet where the light path was leading. The overall system length was limited to approx. 70 cm, including the camera's body. The position of the light splitter was defined by the geometry of the mechanics. It was decided not to place any optics inside the vacuum tank.

Two new CCD type sensors were considered: an EM (Electron Multiplied) CCD and an EB (Electron Bombarded) CCD providing light amplification. It was needed to tilt the EB CCD by 90° (see Fig. 2).

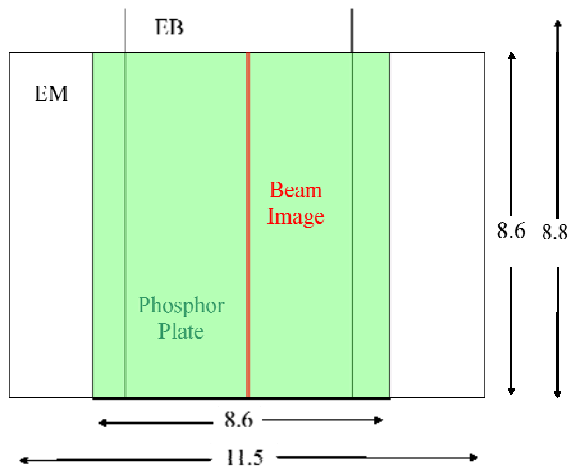

Figure 2: Size and orientation of EM and EB CCDs.

Focusing of the system had to be possible in a reasonable range and the designed optics had to fit inside the C-mount system and have a reasonable cost.

The numerical aperture in the image plane had to be reasonably restricted, because the CCD elements do not accept rays at high angles.

The imaging aberrations should be kept below 1% with respect to the measured transverse beam size.

DESIGN COCNCEPT AND STARTING POINT FOR OPTIMIZATION

Two commercially available doublets are placed between the vacuum window of the detector and the splitting prism with an aperture stop amid. Magnification of this part is matched to the MAPMT and no more lenses are used downstream the splitter. The doublets are optimized for the infinite object position, but as the light

rays are exiting the first lens almost parallel, it has to be used in the opposite direction.

An objective is placed between the splitter and the CCD in the straight path to match the magnification to the smaller square's diagonal of the EM CCD. The objective lenses were supposed to be produced on customer order.

The 150 year old Petzval design with 2 positive power doublets was used as the starting point for the optimization.

OPTIMIZATION AND FINAL DESIGN

Optimization of an optical design required a merit function incorporating target values and constraints of the system. The major part of this function was generated by the ZEMAX program optimizing mainly the RMS spot size for the defined image points and a range of wavelengths 520 – 580nm with a maximum weight at 550nm. A higher number of dimensional constraints had to be carefully set and progressively modified with the optimization evolution. Only reasonable glasses and shapes were used.

During optimization, the first lens of the objective was found not to be crucial for the performance and optimization continued with only three lenses.

The diameter and length of the last element were found to be the major constraint, because it had to fit inside the C-mount and be mechanically hooded outside of it.

Because of mounting difficulties, the front surface of the last element (Fig. **3**) was chosen to be flat without any important losses of image quality. The whole group has a possibility of focalization by its axial movement.

The final design consists of two Optosigma© doublets (200.1 and 169.8mm focal length), a diaphragm almost in the middle of them and an objective (3 elements in one group). Due to supplier stock problems, the first and second elements are made of SK16 glass, the last of SF14.

The main merit target concerned the x component of the RMS image spot; because only one contributes to the resolution of the beam's image (summing the lines along the y coordinate). One can see (Fig. **5**) that the achieved resolution (RMS spot size in the image space) varied from 25μm in the image centre to 37μm at the edges.

Geometrical distortion was also one of the merit function constraints, because it could contribute to the systematic error. One can see a maximum distortion of 2.4%, but actually the beam image should never be in that region. Moreover, this is the maximum deviation from linear imaging and is almost constant for the whole image column (with a small beam) and by summing the lines one gets just a position error.

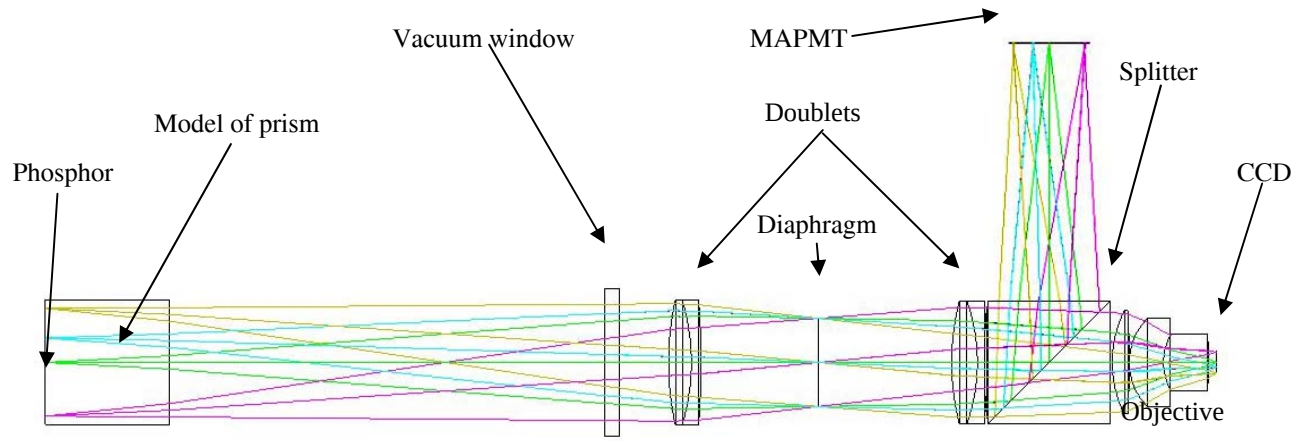

Figure 3: Designed imaging system with optical paths for two separated detectors

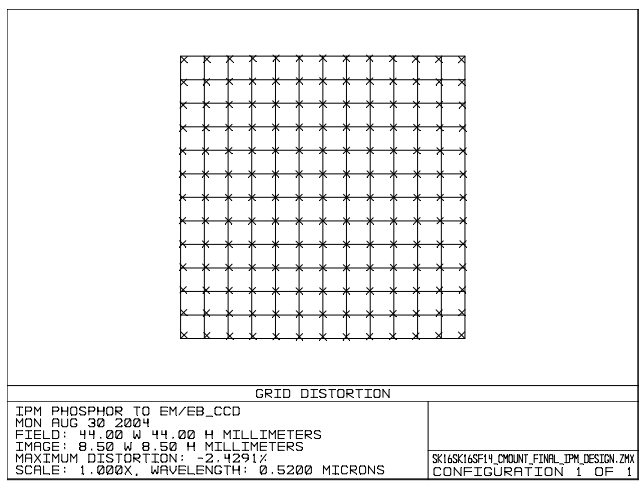

Figure 4: Geometrical distortion of an ideal grid imaged to the CCD.

IMAGING PERFORMANCES AND MEASUREMENTS

Several parameters related with imaging performances were simulated in the Zemax optical CAD program.

The geometrical distortion (Fig. 4) is an important aberration which could have serious impact on the profile measurement precision. The barrel distortion of the system is present mainly in the image corners, where the beam image should normally not be present.

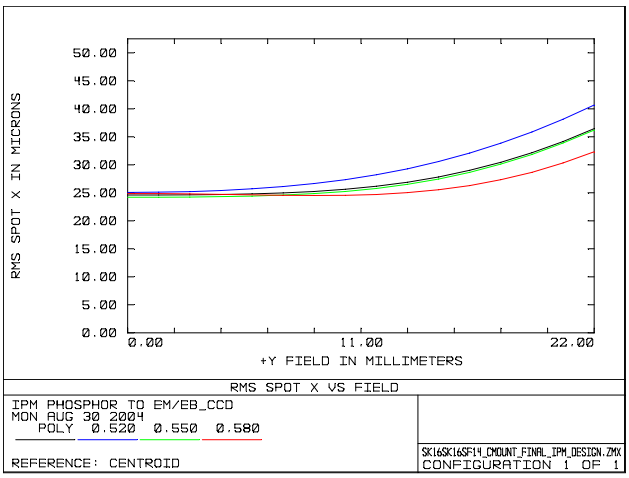

Figure 5: RMS spot size (x component) for different wavelengths.

The spot size of an ideal point imaged to the CCD is the main contribution to the systematic error of the optical part of the detector. It was minimized to a reasonable level (Fig. 5) considering the space requirements. The systematic error caused by the nonzero image of a spot is summarized in the Tab. 1 for different beam sizes and image regions.

Table 1: Calculated systematic errors of measured beam size for different energies.

Average beam size in SPS	**2.3mm (26GeV)**	**0.6mm (450GeV)**
Expected beam size on CCD	439 μm	141 μm
Max RMS spot size	37 μm	37 μm
Measured beam size	441 μm	146 μm
Relative error (max)	**0.36%**	**3.3%**
Min RMS spot size	25 μm	25 μm
Measured beam size	439.7 μm	143.2 μm
Relative error (min)	**0.16%**	**1.5%**

All the elements of the designed system were produced and mounted during the year 2004. The major problem of the optical setup was its very short distance between the last lens of the objective and the CCD's window due to the production tolerances, so the camera's mounting had to be slightly modified.

The BIPM was successfully installed in the LSS5 in the SPS and tested with LHC beams. The measurements showed an important improvement of the detector's accuracy with respect to the previous year (Fig. 6). The measured beam size was compared with the corresponding wire scanner data. The encouraging results were obtained also thanks to the increased transmission bandwidth of the image acquisition chain.

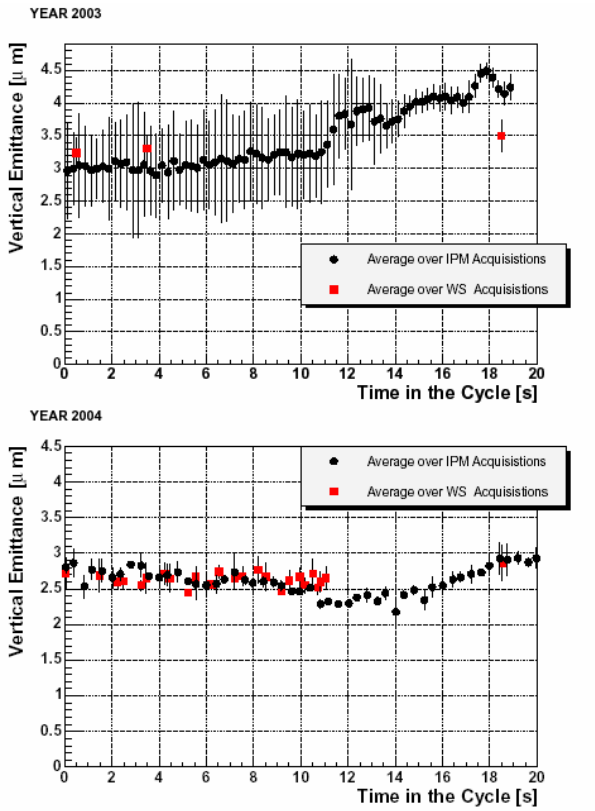

Figure 6: IPM acquisitions with nominal LHC beam and comparison with wire scanners.